



ELSEVIER

Physica D 132 (1999) 373–391

PHYSICA D

www.elsevier.com/locate/physd

Pulses, fronts and oscillations of an elastic rod

Joceline Lega*, Alain Goriely

Department of Mathematics and Program in Applied Mathematics, University of Arizona, Building No. 89, Tucson, AZ 85721, USA

Received 29 January 1999; accepted 26 February 1999

Communicated by A.C. Newell

Abstract

Two coupled nonlinear Klein–Gordon equations modeling the three-dimensional dynamics of a twisted elastic rod near its first bifurcation threshold are analyzed. First, it is shown that these equations are Hamiltonian and that they admit a two-parameter family of traveling wave solutions. Second, special solutions corresponding to simple deformations of the elastic rod are considered. The stability of such configurations is analyzed by means of two coupled nonlinear Schrödinger equations, which are derived from the nonlinear Klein–Gordon equations in the limit of small deformations. In particular, it is shown that periodic solutions are modulationally unstable, which is consistent with the looping process observed in the writhing instability of elastic filaments. Third, numerical simulations of the nonlinear Klein–Gordon equations suggesting that traveling pulses are stable, are presented. ©1999 Elsevier Science B.V. All rights reserved.

Keywords: Elastic rods; Amplitude equations; Nonlinear Klein–Gordon equations; Nonlinear Schrödinger equations

1. Introduction

The study of elastic deformations in rods has a long tradition in mathematics, physics and engineering, dating back to Euler. The main challenge is to understand the different possible shapes elastic rods can conform into under a variety of external stresses. The classical approach to solve such problems is to consider the different static equilibria of rods and study through variational principles the bifurcation between them [1,2]. The dynamical problem, namely how different configurations evolve in time or change to one another is not usually addressed. Another, closely related, classical problem in the theory of elasticity is the propagation of waves in elastic media. In thin elastic rods, it is known that two types of waves can exist: they are *flexural* and *torsional* waves and propagate variation of curvature and twist along the rod. Roughly speaking, the former can be obtained by suddenly moving one end of a long straight rod while the latter can result from a sudden twist of one end of the filament. Both aspects, structural deformations under stress and wave propagation, can be studied together by considering the dynamics of elastic rods. A convenient setting for such a study is provided by the Kirchhoff model for thin elastic filaments.

* Corresponding author. E-mail: lega@math.arizona.edu.

In this paper we study some aspects of the dynamics of elastic rods. As shown in [3], the Kirchhoff model can be used to analyze the stability (with respect to change of tension or twist) of straight twisted rods under tension. Near the first bifurcation point, that is when straight twisted filaments lose their stability, the rod dynamics may be described by two amplitude equations, which were derived by Goriely and Tabor in [3]. These equations take the form of two nonlinear Klein–Gordon equation describing the coupling of twist density to amplitude of deformation. This paper is devoted to an analysis of these amplitude equations, and is organized as follows. In Section 2, we briefly describe the Kirchhoff model. The amplitude equations for the near-threshold dynamics are given in Section 3, where we also discuss their scalings, symmetries and Hamiltonian nature. Section 4 is devoted to the analysis of traveling wave solutions and to simple configurations of the elastic filament. Section 5 discusses the reduction of the coupled Klein–Gordon equations to two coupled nonlinear Schrödinger equations, which are valid in the limit of small deformations. Solutions to the latter system are then compared to those of the former, and the stability of some simple traveling wave solutions is thereby inferred. Section 6 shows numerical simulations of the amplitude equations, which suggest that pulses may propagate in a stable fashion. Conclusions are given in Section 7.

2. The Kirchhoff model

The Kirchhoff model describes the dynamics of a free elastic filament in three dimensions. Assuming that the filament is thin (its cross-section is much smaller than its length) and weakly bent (its curvature radius is, at all points, much shorter than its length), a one-dimensional theory can be derived where forces and moments are averaged over cross-sections perpendicular to the central axis of the filament. This allows to describe the dynamics in terms of two independent variables, namely time and arc-length (respectively, x and t). The forces and moments exerted on a cross-section of the filament are then written in a local basis, attached to the central axis $\mathcal{X} = \mathcal{X}(x, t)$, which is similar to the Frenet frame. This director basis $\{\mathbf{d}_1, \mathbf{d}_2, \mathbf{d}_3\}$ is a right-handed orthonormal basis built by taking \mathbf{d}_3 as the tangent vector to the axis, $\mathbf{d}_3(x, t) = d\mathcal{X}/dt$, and \mathbf{d}_1 as the vector following the elastic twist in the plane normal to the central axis. Since the curve $\mathcal{X} = \mathcal{X}(x, t)$ can be obtained by integrating the tangent vector $\mathbf{d}_3(x, t)$, i.e., $\mathcal{X}(x, t) = \int^s \mathbf{d}_3(s, t) ds$, the space and time evolution of the director basis specifies the kinematics of the filament.

As a consequence of the orthonormality of the director basis $\{\mathbf{d}_1, \mathbf{d}_2, \mathbf{d}_3\}$, we can write

$$\mathbf{d}'_i = \boldsymbol{\kappa} \times \mathbf{d}_i, \quad \dot{\mathbf{d}}_i = \boldsymbol{\omega} \times \mathbf{d}_i, \quad i = 1, 2, 3. \quad (1)$$

where $(\)$ and $(\)'$ stand, respectively, for derivatives with respect to time and arc-length. The vectors $\boldsymbol{\kappa}$ and $\boldsymbol{\omega}$ are called the *twist* and *spin vectors*. They can be written as $\boldsymbol{\kappa} = \sum_{i=1}^3 \kappa_i \mathbf{d}_i$ and $\boldsymbol{\omega} = \sum_{i=1}^3 \omega_i \mathbf{d}_i$. The dynamics of the filament depends on the total force and moment, $\mathbf{F} = \mathbf{F}(s, t)$ and $\mathbf{M} = \mathbf{M}(s, t)$, experienced by the elastic rod. In terms of the director basis, these vectors read $\mathbf{F} = \sum_{i=1}^3 f_i \mathbf{d}_i$, $\mathbf{M} = \sum_{i=1}^3 M_i \mathbf{d}_i$. The Kirchhoff model combines conservation of linear and angular momentum with the constitutive relationship of linear elasticity, which relates moments to strains, characterized by the twist vector. For a naturally straight rod (i.e., without intrinsic curvature or twist) with circular cross-section, the scaled Kirchhoff equations read [4,5]:

$$\mathbf{F}'' = \ddot{\mathbf{d}}_3, \quad (2.a)$$

$$\mathbf{M}' + \mathbf{d}_3 \times \mathbf{F} = \mathbf{d}_1 \times \dot{\mathbf{d}}_1 + \mathbf{d}_2 \times \dot{\mathbf{d}}_2, \quad (2.b)$$

$$\mathbf{M} = \kappa_1 \mathbf{d}_1 + \kappa_2 \mathbf{d}_2 + \Gamma \kappa_3 \mathbf{d}_3, \quad (2.c)$$

where $\Gamma = 1/(1 + \sigma)$ (σ is the Poisson ratio) measures the ratio between the bending and twisting coefficients of the rod. In typical elastic material the Poisson ratio σ varies between 1/2 and 0, that is, Γ varies between 2/3 and

1. Equations (2.a), (2.b) and (2.c), together with Eq. (1), can be reduced to a set of nine second order equations in space and time, for the nine unknowns $(\boldsymbol{\kappa}, \boldsymbol{\omega}, \mathbf{F})$.

3. Amplitude equations, scalings and Hamiltonian formalism

3.1. Amplitude equations

The stability of a given stationary filament parameterized by $(\boldsymbol{\kappa}^{(0)}, \boldsymbol{\omega}^{(0)}, \mathbf{f}^{(0)})$ can be obtained by expanding all quantities up to first order in a small perturbation parameter ϵ and requiring that the basis remains orthonormal to each order [6]:

$$\mathbf{d}_i = \mathbf{d}_i^{(0)} + \epsilon \boldsymbol{\alpha} \times \mathbf{d}_i^{(0)} + O(\epsilon^2), \tag{3.a}$$

$$\boldsymbol{\kappa} = \boldsymbol{\kappa}^{(0)} + \epsilon [(\boldsymbol{\alpha}^{(1)})' + \boldsymbol{\kappa}^{(0)} \times \boldsymbol{\alpha}^{(1)}] + O(\epsilon^2), \tag{3.b}$$

$$\boldsymbol{\omega} = \dot{\boldsymbol{\alpha}}^{(1)} + O(\epsilon^2), \tag{3.c}$$

$$\mathbf{F} = \sum_i [f_i^{(0)} + \epsilon (f_i^{(1)} + (\boldsymbol{\alpha} \times \mathbf{f}^{(0)})_i)] \mathbf{d}_i^{(0)} + O(\epsilon^2). \tag{3.d}$$

Inserting these expressions in the Kirchhoff equations and collecting the terms to first order in ϵ , a linear equation can be obtained for $\mathbf{m} = (\boldsymbol{\alpha}^{(1)}, \mathbf{f}^{(1)})$:

$$L_E(\boldsymbol{\kappa}^{(0)}, \mathbf{f}^{(0)}) \cdot \mathbf{m} = 0, \tag{4}$$

where L_E is a linear, second-order differential operator in s and t , whose coefficients depend on s through the unperturbed solution $(\boldsymbol{\kappa}^{(0)}, \mathbf{f}^{(0)})$. Its explicit form can be found in [7]. For the case of the twisted straight rod under tension, the stationary solution is simply given by

$$\boldsymbol{\kappa}^{(0)} = (0, 0, \gamma), \quad \mathbf{f}^{(0)} = (0, 0, P^2). \tag{5}$$

Solutions to Eq. (4) can be expressed as the sum of fundamental modes of the form:

$$\mathbf{m} = e^{\sigma t} (A \boldsymbol{\xi}_n e^{inx} + A^* \boldsymbol{\xi}_n^* e^{-inx}), \tag{6}$$

where $\boldsymbol{\xi} \in \mathbb{C}^6$ and the growth rate σ is related to the mode n by the dispersion relation, $\Delta(\sigma, n) = 0$, obtained by substituting Eq. (6) into Eq. (4). The neutral curves are the curves in parameter space for which stationary solutions exist. They are obtained by solving $\Delta(0, n) = 0$, which reads:

$$(\gamma^2 - n^2)[(\gamma^2(\Gamma - 1) - P^2 - n^2)^2 - \gamma^2(\Gamma - 2)^2 n^2] = 0. \tag{7}$$

The analysis of this dispersion relation reveals that the straight infinite twisted pulled rod becomes unstable for $\gamma_c = \pm 2P/\Gamma$. This relation is known in elasticity theory as *Love's criterion*. For this value, a stationary solution can be written as

$$\mathbf{m} = B \boldsymbol{\xi}_0 + A \boldsymbol{\xi}_{n_c} e^{in_c x} + A^* \boldsymbol{\xi}_{n_c}^* e^{-in_c x} + \dots, \tag{8}$$

where the dots stand for higher order corrections and $n_c = P(2 - \Gamma)/\Gamma$,

$$\boldsymbol{\xi}_0 = (0, 0, 1, 0, 0, 1), \quad \boldsymbol{\xi}_{n_c} = (1, i, 0, -iP^2, P^2, 0). \tag{9}$$

For fixed P , the straight rod becomes unstable at the critical twist γ_c and evolves towards a configuration which, to first order, is a helical filament and reads:

$$\mathcal{X} = \left(x, \frac{2A}{P} \cos xP, \frac{2A}{P} \sin xP \right) + \dots \quad (10)$$

Near threshold, the nonlinear dynamics of the filament is described by the following amplitude equations [7]:

$$\frac{P^2 + 1}{P^2} \frac{\partial^2 A}{\partial t^2} - \frac{\partial^2 A}{\partial x^2} = P\Gamma A \left(E - 2P|A|^2 + \frac{\partial B}{\partial x} \right), \quad (11.a)$$

$$\frac{2}{\Gamma} \frac{\partial^2 B}{\partial t^2} - \frac{\partial^2 B}{\partial x^2} = -2P \frac{\partial |A|^2}{\partial x}. \quad (11.b)$$

In this nonlinear analysis, $B = B(x, t)$ and $A = A(x, t)$ represent, respectively, the slowly-varying amplitudes of the axial twist and the unstable helical mode. For given solutions A and B of Eqs. (11.a) and (11.b), the shape and motion of the filament in space is obtained by integrating the tangent vector. To second order, the filament shape is given by:

$$\mathcal{X}(x, t) = \left(\begin{array}{c} \int (1 - 2|A|^2) dx \\ \int [-\cos(Px)(2\operatorname{Re}(A) + B\operatorname{Im}(A)) - \sin(Px)(2\operatorname{Im}(A) - B\operatorname{Re}(A))] dx \\ \int [-\sin(Px)(2\operatorname{Re}(A) + B\operatorname{Im}(A)) + \cos(Px)(2\operatorname{Im}(A) - B\operatorname{Re}(A))] dx \end{array} \right). \quad (12)$$

The rest of this paper is devoted to the analysis of these solutions and its consequences for the dynamics of rods.

3.2. Scalings

To keep the discussion as general as possible and to reduce the number of free parameters, it is convenient to re-write the amplitude equations in terms of scaled quantities. If we make the changes of variables

$$t = \sqrt{\frac{2}{\Gamma}} Lt', \quad x = Lx', \quad A = \frac{\sqrt{P^2 + 1}}{(2LP^2)} A', \quad B = \frac{(P^2 + 1)}{(2P^3L)} B', \quad (13)$$

Eqs. (11.a) and (11.b) become, after dropping the primes,

$$\frac{\partial^2 A}{\partial t^2} - c_0^2 \frac{\partial^2 A}{\partial x^2} = \mu A - |A|^2 A + \frac{\partial B}{\partial x} A, \quad (14.a)$$

$$\frac{\partial^2 B}{\partial t^2} - \frac{\partial^2 B}{\partial x^2} = -\frac{\partial |A|^2}{\partial x}, \quad (14.b)$$

where

$$c_0^2 = \frac{2P^2}{\Gamma(P^2 + 1)} \quad \text{and} \quad \mu = \frac{2EP^3L^2}{P^2 + 1}. \quad (15)$$

Only two parameters are left. The first one, μ , measures the linear growth rate of perturbations to the solution $A = 0$ in the absence of B . The second one, c_0 , is the ratio v_A/v_B of the group velocities v_A and v_B describing the speed at which perturbations of A and B propagate. These scaled equations provide a convenient way of analyzing the dynamics and the solutions of Eqs. (11.a) and (11.b), and most of the discussion below will refer to them. The new space scale depends on L , a characteristic length scale of the problem. For a finite rod, we take L as the total length of the elastic filament. In what follows, we refer to these equations as the coupled nonlinear Klein–Gordon

(CNLKG) equations. Similar CNLKG equations appear in a variety of fields such as plasma physics (See [8]; p. 318), partial difference equations [9], baroclinic instabilities [10], or more generally as amplitude equations for dispersive systems [11].

3.3. Hamiltonian form

From the scaled form (14.a) and (14.b), it is straightforward to see that the coupled Klein–Gordon equations can be written in Hamiltonian form

$$\frac{\partial A}{\partial t} = \frac{\delta H}{\delta \bar{u}}, \quad \frac{\partial u}{\partial t} = -\frac{\delta H}{\delta \bar{A}}, \tag{16.a}$$

$$\frac{\partial B}{\partial t} = \frac{\delta H}{\delta v}, \quad \frac{\partial v}{\partial t} = -\frac{\delta H}{\delta \bar{B}}, \tag{16.b}$$

where δ refers to the Fréchet derivative,

$$u = \frac{\partial A}{\partial t}, \quad v = \frac{\partial B}{\partial t}, \tag{17}$$

and $H = \int h(x, t) dx$ with

$$h(x, t) = c_0^2 \left| \frac{\partial A}{\partial x} \right|^2 - \mu |A|^2 + \frac{1}{2} |A|^4 - |A|^2 \frac{\partial B}{\partial x} + \left| \frac{\partial A}{\partial t} \right|^2 + \frac{1}{2} \left(\frac{\partial B}{\partial x} \right)^2 + \frac{1}{2} \left(\frac{\partial B}{\partial t} \right)^2. \tag{18}$$

The integral is taken over the real line if $h(x, t)$ is $L^1[(-\infty, +\infty)]$. If A does not vanish at infinity, the integration is taken on a suitable box (for instance, one period of the solution for periodic solutions).

3.4. Symmetries

Equations (14.a) and (14.b) have a few symmetries that can be used to simplify our analysis of special solutions. Below, we assume that $a_0(s, \tau)$ and $b_0(s, \tau)$ are solutions to Eqs. (14.a) and (14.b). The solutions $A(x, t)$ and $B(x, t)$ are obtained by applying the indicated symmetries to a_0 and b_0 .

1. Space translation invariance:

$$A(x, t) = a_0(x + x_0, t), \quad B(x, t) = b_0(x + x_0, t), \tag{19}$$

where x_0 is a real arbitrary constant.

2. Time translation invariance:

$$A(x, t) = a_0(x, t + t_0), \quad B(x, t) = b_0(x, t + t_0), \tag{20}$$

where t_0 is a real arbitrary constant.

3. Uniform shift on B

$$A(x, t) = a_0(x, t), \quad B(x, t) = b_0(x, t) + \chi, \tag{21}$$

where χ is a real arbitrary constant. This transformation corresponds to a uniform rotation of the local frame of reference $(\mathbf{d}_1, \mathbf{d}_2, \mathbf{d}_3)$ about the tangent vector to the elastic rod \mathbf{d}_3 , and is not physically relevant.

4. Gauge invariance:

$$A(x, t) = a_0(x, t)\exp(i\phi), \quad B(x, t) = b_0(x, t), \quad (22)$$

where ϕ is a real arbitrary constant. This transformation corresponds to a uniform translation of the periodic solution of envelope A and is due to the invariance of the Kirchoff equations with respect to space-time translations before bifurcation.

5. Space reflection symmetry

$$A(x, t) = a_0(-x, t), \quad B(x, t) = -b_0(-x, t). \quad (23)$$

6. Time reflection symmetry

$$A(x, t) = a_0(x, -t), \quad B(x, t) = b_0(x, -t), \quad (24)$$

which is due to the fact that the original system is time reversible.

7. Dilation invariance:

$$A(x, t) = \alpha a_0(\alpha x, \alpha t), \quad B(x, t) = \alpha b_0(\alpha x, \alpha t) + \frac{\mu}{\alpha^2 - 1}x, \quad (25)$$

where α is a real arbitrary constant. This transformation is due to the fact that adding a linear term in x to B renormalizes the growth rate μ , which in turn can be changed back to its initial value by scaling space, time, and the envelopes A and B .

Whereas the Hamiltonian is preserved by transformations 1 to 6, the dilation 7 does not conserve H . Since the amplitude Eqs. (11.a) and (11.b) have been derived by assuming that the solution \mathbf{m} defined in Section 2 remains bounded at infinity, we will set α so that B tends to a constant at infinity. This condition turns out to be necessary for H to remain bounded.

4. Traveling waves solutions of CNLKG

We now look for a two-parameter family of solutions of the form:

$$A = a(\xi)e^{i\omega t}, \quad B = b(\xi), \quad (26)$$

where $\xi = x - ct$. This family includes periodic stationary solutions ($c = \omega = 0$), oscillatory periodic solutions ($c = 0$), homogeneous solutions (a, b constant, $c = \omega = 0$), plane waves (b, ω and $|A|$ constant), non-oscillating traveling waves solutions and pulses ($\omega = 0$). The general case where both c and ω do not vanish correspond to traveling waves. These solutions periodically oscillate in time as they travel at constant speed c . Together with Eq. (26), Eqs. (14.a) and (14.b) read (where primes denotes ξ -derivatives)

$$(c^2 - c_0^2)a'' + 2ic\omega a' = a(\omega^2 + \mu - |a|^2 + b'), \quad (27.a)$$

$$(c^2 - 1)b'' = -(|a|^2)'. \quad (27.b)$$

The last equations can be integrated once to yield $(c^2 - 1)(b' - K_1) = -|a|^2$. We then use the expression for b' to simplify Eq. (27.a)

$$(c^2 - c_0^2)a'' + 2ic\omega a' = a \left(\omega^2 + \mu + K_1 - \frac{c^2}{(c^2 - 1)}|a|^2 \right). \quad (28)$$

In order to obtain a set of real differential equations, we set $a = R(\xi)e^{i\theta(\xi)}$, which gives

$$(c^2 - c_0^2)R'' = R \left(\omega^2 + \mu + K_1 - 2c\omega\Theta + (c^2 - c_0)^2\Theta^2 - \frac{c^2}{(c^2 - 1)}R^2 \right), \tag{29.a}$$

$$2 \left(\Theta - \omega \frac{c}{(c^2 - c_0^2)} \right) R' + R\Theta' = 0, \tag{29.b}$$

where $\theta' = \Theta$. The system for (R, Θ) has two first integrals:

$$H = \frac{1}{2}(R')^2 + \frac{1}{2} \left(\Theta^2 - \frac{(\mu + K_1 + \omega^2)}{c\omega} \Theta \right) R^2 + \frac{c^2 R^4}{4(c^2 - 1)(c^2 - c_0^2)}, \tag{30.a}$$

$$G = ((c^2 - c_0^2)\Theta - \omega c)R^2. \tag{30.b}$$

The first integral G is reminiscent of Kepler’s second law for the motion of a particle in a central force field. It can be used to simplify H as follows:

$$H_1 = H + G \frac{\omega^2(c^2 + c_0^2) - (\mu + K_1)(c^2 - c_0^2)}{2c\omega(c^2 - c_0^2)^2} = \frac{1}{2}(R')^2 + \frac{G^2}{2(c^2 - c_0^2)^2}R^{-2} + \frac{\omega^2 c_0^2 - (\mu + K_1)(c^2 - c_0^2)}{2(c^2 - c_0^2)^2}R^2 + \frac{c^2}{4(c^2 - 1)(c^2 - c_0^2)}R^4. \tag{31}$$

Thus, H_1 is an Hamiltonian describing the motion of a particle in a one-dimensional *effective potential* $V_{\text{eff}} = H_1 - (R')^2/2 = v_{-2}R^{-2} + v_2R^2 + v_4R^4$. This reduced Hamiltonian system can be solved through the change of variables

$$\xi = \beta\zeta, \quad z = -v_4R^2, \tag{32}$$

which transforms the Hamiltonian H_1 into the standard form:

$$\left(\frac{dz}{dt} \right)^2 = \frac{4}{z_3 - z_1} (z - z_1)(z_2 - z)(z_3 - z), \tag{33}$$

where $\beta^{-1} = \sqrt{2(z_3 - z_1)}$ and

$$z_1 + z_2 + z_3 = v_2, \quad z_1z_2 + z_2z_3 + z_3z_1 = -v_4H_1, \quad z_1z_2z_3 = v_4^2v_{-2}^2. \tag{34}$$

The general solution of Eq. (33) is $z = z_1 + (z_2 - z_1)\text{sn}^2(\zeta|k)$ where $k^2 = (z_2 - z_1)/(z_3 - z_1)$. That is,

$$R = \sqrt{\frac{z_1 + (z_2 - z_1)\text{sn}^2(\beta\xi|k)}{v_4}}. \tag{35}$$

The conditions for the roots z_1, z_2, z_3 to be real is:

$$27v_{-2}^4v_4^2 + 2H_1(9v_2v_{-2}^2 - 2H_1^2)v_4 - v_2^2H_1^2 + 4v_2^3v_{-2}^2 < 0. \tag{36}$$

The first integral G can then be used to give an explicit form of the angular coordinate θ in terms of incomplete elliptic integrals of the third kind. Explicit forms for the periods of given periodic orbits can be obtained in a similar fashion.

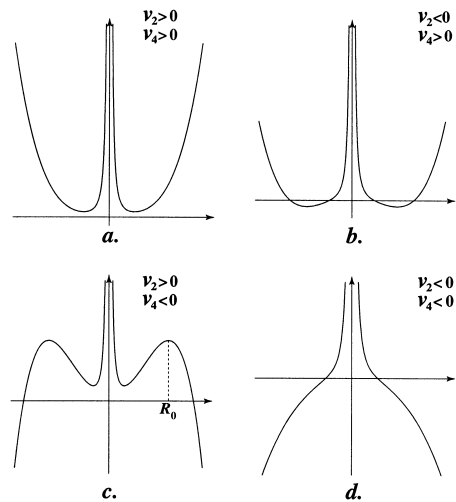


Fig. 1. Different shapes of the effective potential V_{eff} as a function of R when $G \neq 0$.

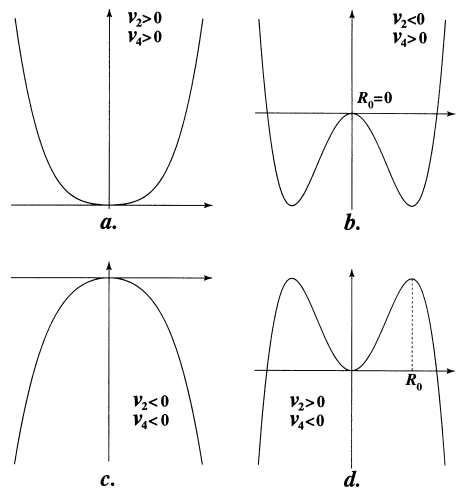


Fig. 2. Different shapes of the effective potential V_{eff} as a function of R when $G = 0$.

To understand the different types of orbits that the system H_1 may exhibit it is easier to study the potential V_{eff} directly. There are two main cases that can be distinguished depending on whether G vanishes or not. In each case, four different potential shapes can be obtained (depending on the sign of the coefficients v_2, v_4). These potentials are shown, respectively, in Figs. 1 and 2.

We now focus on localized solutions, that is solutions for which the amplitudes A and B tend asymptotically to a constant and vary rapidly in a finite region. At the level of the Hamiltonian system with Hamiltonian H_1 , we look for homoclinic and heteroclinic orbits connecting the fixed point R_0 to himself (homoclinic case) or to $-R_0$ (heteroclinic case). In both cases, we choose the constant K_1 to ensure that $\lim_{\xi \rightarrow \pm\infty} b' = 0$, that is $K_1 = R_0^2 / (c^2 - 1)$. Analytic expressions will be given with a minimum number of free parameters. More general solutions can be obtained by using the symmetries discussed in Section 3.4.

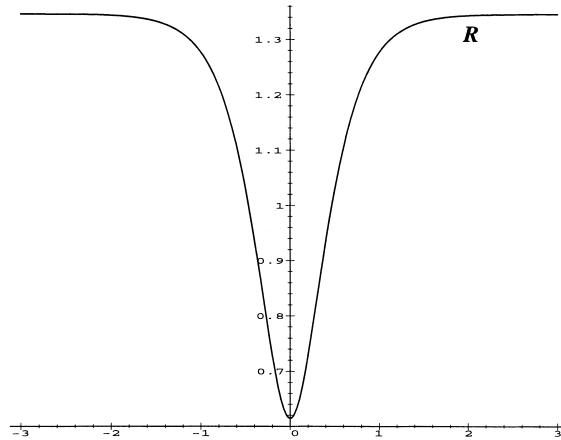


Fig. 3. A traveling hole solution ($v_2 = 4, v_4 = -1, v_{-2} = -5, c_0 = 3, \omega = 0$).

4.1. Traveling holes

If $G \neq 0$, the only possible localized solutions occur for $v_2 > 0$ and $v_4 < 0$. These orbits are, for the Hamiltonian H_1 , homoclinic to the fixed point R_0 (See Fig. 1(c)). In this case, one sets $0 < z_1 < z_2 = z_3 = -v_4 R_0^2$ in Eq. (35) to obtain:

$$R^2 = R_0^2 - \alpha^2 \operatorname{sech}^2(\beta\xi), \tag{37}$$

where

$$\beta^2 = -6v_4 R_0^2 - 2v_2 \quad \text{and} \quad \alpha^2 = \frac{(3v_4 R_0^2 + v_2)}{v_4}. \tag{38}$$

The fixed point R_0 is the largest root of $2z^6 + v_2 z^4 - v_{-2}^2 = 0$. The homoclinic orbit exists when $H_1 = R_0^2(2v_2 + 3v_4 R_0^2)$. Explicit forms of $\theta = \theta(\xi)$ and $b = b(\xi)$ can be obtained in terms of elementary functions. A typical traveling hole amplitude profile is shown in Fig. 3.

4.2. Traveling pulses

Traveling pulses exist when $G = 0, v_2 < 0$ and $v_4 > 0$ (Fig. 2(b)). They correspond to orbits of the reduced Hamiltonian system which are homoclinic to the fixed point $R_0 = 0$, at which $H_1 = 0$. They read:

$$a = \alpha \operatorname{sech}(\beta\xi) \exp\left(i \frac{\omega c}{c^2 - c_0^2} \xi\right). \tag{39.a}$$

$$b = \frac{\alpha^2}{\beta(1 - c^2)} \tanh(\beta\xi), \tag{39.b}$$

where

$$\alpha^2 = \frac{2(c^2 - 1)}{c^2(c^2 - c_0^2)} (\mu(c^2 - c_0^2) - \omega^2 c_0^2) \quad \text{and} \quad \beta^2 = \frac{\mu(c^2 - c_0^2) - \omega^2 c_0^2}{(c^2 - c_0^2)^2}. \tag{40}$$

This solution exists whenever $\alpha^2 > 0$ and $\beta^2 > 0$. Typical profiles of A and B are shown in Fig. 4, and the corresponding filament is depicted in Fig. 5.

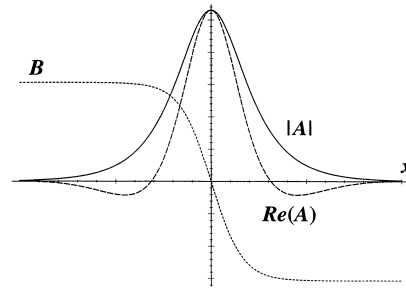


Fig. 4. A traveling pulse ($\mu = 1/4, c = 2, c_0 = \sqrt{2}, \omega = 1/4, \Gamma = 3/4$).

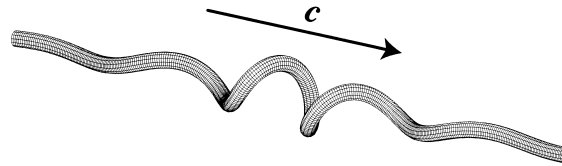


Fig. 5. Filament corresponding to the homoclinic solution of Fig. 3.

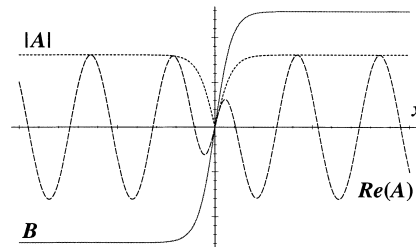


Fig. 6. A heteroclinic solution ($\mu = 1/2, c = 6/5, c_0 = 3/2, \omega = 10, \Gamma = 3/4$).

4.3. Fronts

There exists yet another localized solution when $G = 0$. If $v_2 > 0$ and $v_4 < 0$ the Hamiltonian H_1 accommodates heteroclinic orbits (See Fig. 2(d)), given by

$$a = \alpha \tanh(\beta\xi) \exp\left(i \frac{\omega c}{c^2 - c_0^2} \xi\right), \tag{41.a}$$

$$b = \frac{\alpha^2}{\beta(c^2 - 1)} \tanh(\beta\xi), \tag{41.b}$$

where

$$\alpha^2 = \frac{(c^2 - 1)(\mu(c^2 - c_0^2) - \omega^2 c_0^2)}{(2c^2 - 1)(c^2 - c_0^2)} \quad \text{and} \quad \beta^2 = \frac{c^2(\omega^2 c_0^2 - \mu(c^2 - c_0^2))}{2(2c^2 - 1)(c^2 - c_0^2)^2}. \tag{42}$$

Such a solution, referred to as a front, is depicted in Figs. 6 and 7.

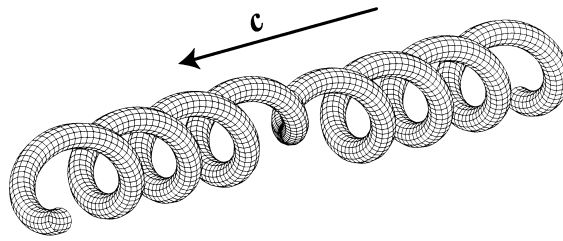


Fig. 7. The filament corresponding to the front solution of Fig. 5.

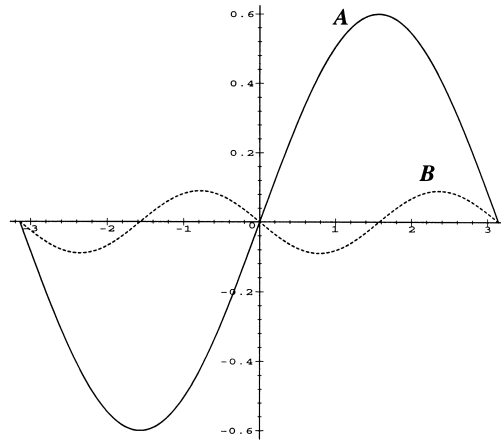


Fig. 8. A Periodic solution ($\alpha = 6/10$, $k = 1$, $P = 10$, $\Gamma = 3/4$).



Fig. 9. The stationary periodic solution corresponding to Fig. 7.

4.4. Stationary periodic solutions

We now consider a simple class of stationary solutions to Eqs. (14.a) and (14.b), which are periodic in x . They read

$$A = \alpha \sin(kx), \quad B = \beta \sin(2kx), \tag{43}$$

where

$$\alpha^2 = -2(k^2 c_0^2 - \mu), \quad \beta = \frac{1}{2k}(k^2 c_0^2 - \mu). \tag{44}$$

Since Eq. (43) solves the scaled coupled Klein–Gordon equations, x varies between 0 and 1. We also assume that k is a multiple of $n\pi$ in order to have the same values of A and B at $x = 0$ and $x = 1$. In terms of solutions to the Kirchhoff equations, Eq. (43) corresponds to a helix whose envelope is modulated and vanishes periodically with period $2\pi L/k$. Typical amplitude profiles are given in Fig. 8, and the corresponding filament is shown in Fig. 9.

5. Analysis of CNLKG in the limit of small deformations

In the limit of small deformations, the CNLKG equations (14.a) and (14.b) can be reduced to two coupled nonlinear Schrödinger (NLS) equations, which may then be used to investigate the stability of some of the localized solutions discussed above. In what follows, we derive these coupled NLS equations and compare some of their solutions to those of CNLKG.

5.1. Reduction to two coupled nonlinear Schrödinger equations

The translational and gauge invariances of Eqs. (14.a) and (14.b) may lead to large-scale instabilities (also called *modulational instabilities*), which play an important role in the dynamics of the system. As was shown in [12] for the case of a single wave equation and for solutions which are periodic in time, these instabilities can be analyzed in terms of envelope equations. The latter are derived from the coupled Klein–Gordon equations (14.a) and (14.b) by multiple scales analysis. To understand the scalings involved in the derivation, consider the periodic solutions of CNLKG given by

$$A = Re^{ikx}, \quad k^2 = \frac{\mu}{c_0^2} - \frac{\alpha^2}{2c_0^2}. \quad (45)$$

Near threshold ($\alpha \simeq 0$), the wave vector of solution (45) can be written as

$$k = -\frac{\sqrt{\mu}}{c_0} + q, \quad (46)$$

where q is small compared to $\sqrt{\mu}/c_0$. To order q , the coefficients α and β satisfy

$$\alpha^2 = 4qc_0\sqrt{\mu} + O(q^2), \quad \beta = -qc_0^2 + O(q^2). \quad (47)$$

This suggests to develop a multiple scales analysis where q and β are of order ϵ^2 , and α is of order ϵ . The scale of q implies that the slow space scale is given by $X_2 = \epsilon^2 x$. We take the slow time scale as $T_1 = \epsilon t$ and write

$$A = \epsilon A_1(x, T, X_2) + \epsilon^2 A_2(x, T, X_2) + \epsilon^3 A_3(x, T, X_2) + \dots \quad (48.a)$$

$$B = \epsilon B_1(x, T, X_2) + \epsilon^2 B_2(x, T, X_2) + \epsilon^3 B_3(x, T, X_2) + \dots \quad (48.b)$$

where $T = \epsilon t$, $X_2 = \epsilon^2 x$, and ϵ is a small parameter. As shown in Appendix A, the amplitudes A and B can be written, to order ϵ^3 , as

$$A = F_1(x, t)e^{-i(\sqrt{\mu}/c_0)x} + F_2(x, t)e^{i(\sqrt{\mu}/c_0)x}, \quad (49.a)$$

$$B = \kappa + \frac{ic_0}{2\sqrt{\mu}} \left(F_1(x, t)F_2^*(x, t)e^{-2i(\sqrt{\mu}/c_0)x} - F_2(x, t)F_1^*(x, t)e^{2i(\sqrt{\mu}/c_0)x} \right). \quad (49.b)$$

The envelopes F_1 and F_2 satisfy two solvability conditions obtained at order ϵ^3 (see Appendix A). They take the form of two coupled nonlinear Schrödinger equations for F_1 and F_2 , which read

$$\frac{\partial^2 F_1}{\partial t^2} + 2ic_0\sqrt{\mu}\frac{\partial F_1}{\partial x} + |F_1|^2 F_1 + |F_2|^2 F_1 = 0, \quad (50.a)$$

$$\frac{\partial^2 F_2}{\partial t^2} - 2ic_0\sqrt{\mu}\frac{\partial F_2}{\partial x} + |F_2|^2 F_2 + |F_1|^2 F_2 = 0. \quad (50.b)$$

These equations, known as the *Manakov equations* [13–15], have the symmetry $F_1 \rightarrow F_2^*$ and $F_2 \rightarrow F_1^*$. As shown in [14,15], they are completely integrable and admit a Lax Pair. Their solitary wave solutions are classified in [16] and various perturbations of these equations have been considered for the description of light propagation in birefringent fibers [17] or counterpropagation in Kerr media [18,19] (see also [20] and [21] as well as references therein).

5.2. *Special solutions of the reduced equations*

We now consider particular solutions to the two coupled nonlinear Schrödinger equations (50.a) and (50.b) and compare them to similar solutions of the coupled Klein–Gordon equations.

5.2.1. *Plane waves*

Plane wave solutions to Eqs. (50.a) and (50.b) of the form

$$F_1 = \sqrt{\omega^2 + 2c_0\sqrt{\mu}p} \exp[i(px + \omega t)], \quad F_2 = 0, \tag{51}$$

correspond to plane wave solutions of CNLKG

$$A = R \exp \left[i \left(px + \omega t - \frac{\sqrt{\mu}x}{c_0} \right) \right], \quad B = 0. \tag{52}$$

Indeed, R^2 in Eq. (52) is given by $R^2 = \omega^2 + 2c_0p\sqrt{\mu} - c_0^2p^2 = \omega^2 + 2c_0p\sqrt{\mu} + O(p^2)$, which is consistent with the scaling $p = O(\epsilon^2)$ and the fact that expressions (48.a) and (48.b) are valid at order ϵ^3 .

Since plane wave solutions of Eqs. (50.a) and (50.b) are modulationally unstable, plane wave solutions of CNLKG are also unstable. As a consequence, traveling holes and fronts of CNLKG are unstable since their asymptotic states, which are plane wave solutions, are unstable.

5.2.2. *Stationary solutions*

Stationary solutions to Eqs. (50.a) and (50.b) with $F_1 = R \exp(iqx)$ and $F_2 = F_1^*$ are such that $R^2 = c_0q\sqrt{\mu}$. In terms of A and B , and assuming $\kappa = 0$ (which can always be done by virtue of Symmetry 3 of Section 3.4), these solutions read

$$A = -\alpha \cos \left(\left(\frac{\sqrt{\mu}}{c_0} - q \right) x \right) + O(\epsilon^4), \tag{53.a}$$

$$B = -\beta \sin \left(2 \left(\frac{\sqrt{\mu}}{c_0} - q \right) x \right) + O(\epsilon^4), \tag{53.b}$$

where

$$\alpha^2 = 4c_0q\sqrt{\mu}, \quad \beta = -c_0^2q. \tag{54}$$

If we translate this solution by a quarter of its period (which again is allowed by Symmetry 1 of Section 3.4), we obtain

$$A = -\alpha \cos \left(\left(\frac{\sqrt{\mu}}{c_0} - q \right) x + \frac{\pi}{2} \right) + O(\epsilon^4) = \alpha \sin \left(\left(\frac{\sqrt{\mu}}{c_0} - q \right) x \right) + O(\epsilon^4), \tag{55.a}$$

$$B = -\beta \sin \left(2 \left(\frac{\sqrt{\mu}}{c_0} - q \right) x + \pi \right) + O(\epsilon^4) = \beta \sin \left(2 \left(\frac{\sqrt{\mu}}{c_0} - q \right) x \right) + O(\epsilon^4). \tag{55.b}$$

This is exactly the near-threshold expansion Eqs. (46) and (47) of the periodic solutions (45). Therefore, the latter correspond to solutions of constant amplitude of Eqs. (50.a) and (50.b), with $F_2 = F_1^*$. Since, with $F_2 = F_1^*$, the two coupled equations (50.a) and (50.b) reduce to the self-focusing nonlinear Schrödinger equation

$$\frac{\partial^2 F_1}{\partial t^2} + 2ic_0\sqrt{\mu}\frac{\partial F_1}{\partial x} + 2|F_1|^2 F_1 = 0, \quad (56)$$

the periodic solutions (45) are modulationally unstable near threshold. This suggests that amplitude deformations will focalize in finite time, and is consistent with the results obtained in [22] for the linear stability analysis of the infinite helix which appears above the writhing bifurcation of a twisted elastic rod.

5.2.3. Traveling pulses

Soliton solutions of Eqs. (50.a) and (50.b) of the form

$$F_1 = \sqrt{2\mu}\frac{c_0}{c} \operatorname{sech}\left(\frac{c_0\sqrt{\mu}}{c^2}(x-ct)\right) \exp\left(i\frac{c_0\sqrt{\mu}}{c}t\right), \quad F_2 = 0, \quad (57)$$

correspond to solutions of Eqs. (48.a) and (48.b) with

$$A = \tilde{\alpha} \operatorname{sech}\left(\tilde{\beta}(x-ct)\right) \exp\left[i\left(\tilde{k}(x-ct) + \tilde{\omega}t\right)\right], \quad B = 0, \quad (58)$$

and

$$\tilde{\alpha} = \frac{c_0\sqrt{2\mu}}{c}, \quad \tilde{\beta} = \sqrt{\mu}\frac{c_0}{c^2}, \quad \tilde{k} = -\frac{\sqrt{\mu}}{c_0}, \quad \tilde{\omega} = \sqrt{\mu}\frac{c_0^2 - c^2}{c_0c}. \quad (59)$$

Since $|A| \leq \sqrt{2\mu}c_0/c$ must be small for the coupled nonlinear Schrödinger equations to be valid, solution (57) are valid in the limit of large c . More precisely, since c_0 and $\sqrt{\mu}$ are finite, c should be such that $c^{-1} = O(\epsilon)$. We now compare this solution to traveling pulse solutions of CNLKG. The latter are of the form:

$$A = \alpha \operatorname{sech}(\beta(x-ct)) \exp[i(k(x-ct) + \omega t)], \quad (60.a)$$

$$B = \frac{\alpha^2}{\beta(c^2 - 1)} \tanh[\beta(x-ct)], \quad (60.b)$$

where

$$\alpha^2 = 2\frac{\mu(c^2 - 1)}{c^2} - 2\frac{\omega^2(c^2 - 1)c_0^2}{c^2(c^2 - c_0^2)}, \quad \beta^2 = \frac{\mu}{c^2 - c_0^2} - \frac{c_0^2\omega^2}{(c^2 - c_0^2)^2} \quad (61.a)$$

$$k = \frac{c\omega}{c^2 - c_0^2}. \quad (61.b)$$

With $\omega = \tilde{\omega} = \sqrt{\mu}(c_0^2 - c^2/c_0c)$, the last equation becomes $k = -\sqrt{\mu}/c_0 = \tilde{k}$, and α^2 and β^2 read:

$$\alpha^2 = 2\mu\frac{c_0^2}{c^2} \left[1 - \frac{1}{c^2}\right] = \tilde{\alpha}^2 + O\left(\frac{1}{c^4}\right) = \tilde{\alpha}^2 + O(\epsilon^4), \quad (62.a)$$

$$\beta^2 = \frac{c_0^2\mu}{c^4} + O\left(\frac{1}{c^6}\right) = \tilde{\beta}^2 + O(\epsilon^6). \quad (62.b)$$

In other words, the expressions of α^2 , β^2 and $\tilde{\alpha}^2$ and $\tilde{\beta}^2$ are consistent to lowest order. The fact that the nonlinear Schrödinger equations give $B = 0$ instead of $B = (\alpha^2/\beta(c^2 - 1))\tanh[\beta(x-ct)]$ can be understood as follows.

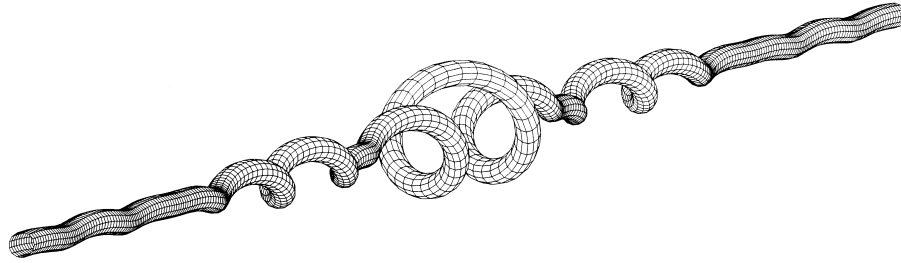


Fig. 10. Shape of the filament corresponding to a double soliton solution of the coupled nonlinear Schrödinger equations. The parameters used to plot this figure, given in terms of the unscaled equations, are $\Gamma = 0.75$, $P = 3$, $E = 0.1$, $L = 40$, $\kappa = 0$, and $c = 2$.

Traveling pulse solutions of CNLKG are found by solving a differential equation for A and then by solving Eq. (27.b) for b . This amounts to solving

$$B' = \frac{dB}{d\xi} = -\frac{|A|^2}{c^2 - 1} = -\frac{\alpha^2}{c^2 - 1} \frac{1}{\cosh^2(\beta\xi)}, \tag{63}$$

where $\xi = x - ct$. But with the expression of α^2 , we have

$$\frac{\alpha^2}{c^2 - 1} = \frac{2\mu c_0^2}{c^4} = O(\epsilon^4), \tag{64}$$

so that $B' = 0$ at order ϵ^3 , *i.e.* $B = \kappa = \text{constant}$ at order ϵ^3 . Therefore, we conclude that soliton solutions (57) of the coupled nonlinear Schrödinger equations correspond to traveling pulses (39.a) and (39.b) of CNLKG.

5.2.4. Double solitons

The coupled nonlinear Schrödinger equations (50.a) and (50.b) also admit solutions of the form

$$F_1 = \sqrt{\mu} \frac{c_0}{c} \operatorname{sech} \left(\frac{c_0 \sqrt{\mu}}{c^2} (x - ct) \right) \exp \left(i \frac{c_0 \sqrt{\mu}}{c} t \right), \quad F_2 = \overline{F_1}, \tag{65}$$

which correspond, in terms of A and B , to

$$A = 2\sqrt{\mu} \frac{c_0}{c} \operatorname{sech} \left[\frac{c_0 \sqrt{\mu}}{c^2} (x - ct) \right] \cos \left[\frac{\sqrt{\mu}}{c_0} \left(x - \frac{c_0^2}{c} t \right) \right], \tag{66.a}$$

$$B = \sqrt{\mu} \frac{c_0^3}{c^2} \operatorname{sech} \left[\frac{c_0 \sqrt{\mu}}{c^2} (x - ct) \right] \sin \left[\frac{2\sqrt{\mu}}{c_0} \left(x - \frac{c_0^2}{c} t \right) \right]. \tag{66.b}$$

Fig. 10 shows a reconstructed filament with A and B given above.

6. Numerical results

Following the stability analysis presented in this paper, we conclude that traveling holes, fronts and periodic solutions of the coupled Klein–Gordon equations are unstable, at least in systems which are large enough for the modulational instability to develop. On the other hand, traveling pulses are unstable if μ is positive since their asymptotic states ($A = 0$, $B = \kappa$) experience exponential growth, but may be stable for negative values of μ . In this section, we show results of numerical simulations of the original (unscaled) coupled Klein–Gordon equations (11.a)

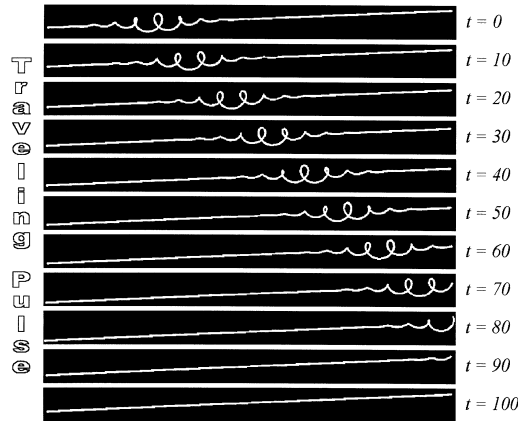


Fig. 11. Numerical simulation of the original (unscaled) nonlinear Klein–Gordon equations, showing the stable propagation of a traveling pulse. Parameters used in the simulation are $\Gamma = 0.75$, $P = 3$, $E = 0.1$, $L = 40$, $\omega = 0$, and $c = 0.6124$.

and (11.b), which suggest that traveling pulses are stable in some parameter regimes. In order to study traveling waves, we designed a code with non-reflecting [23] boundary conditions, which minimize the amount of reflection at the boundaries. The code is second order in time (a typical time-step is $dt = 0.01$) and uses spectral-like finite differences [24] (a typical box length value is $L = 40$, which corresponds to a mesh size $dx = 0.1$). Although no symplectic structure is implemented in the numerics, we checked that the Hamiltonian

$$\mathcal{H} = \int \left[\frac{P^2}{P^2 + 1} \left| \frac{\partial A}{\partial x} \right|^2 + \frac{\Gamma P^4}{P^2 + 1} |A|^4 - \frac{\Gamma P^3}{P^2 + 1} |A|^2 \left(\frac{\partial B}{\partial x} + E \right) + \left| \frac{\partial A}{\partial t} \right|^2 + \frac{\Gamma P^2}{4(P^2 + 1)} \left(\frac{\partial B}{\partial x} + E \right)^2 + \frac{P^2}{2(P^2 + 1)} \left(\frac{\partial B}{\partial t} \right)^2 \right] dx, \quad (67)$$

is conserved to within 0.001% of its value. The simulation has a graphical interface, built with the Advanced Visual Software AVS 5, which allows for interactive change of the parameters.

Fig. 11 illustrates the stable propagation of a traveling pulse (see Eqs. (39.a) and (39.b)), which, in terms of unscaled variables, reads

$$A = \alpha \frac{\sqrt{P^2 + 1}}{2LP^2} \operatorname{sech} \left[\frac{\beta}{L} \left(x - c\sqrt{\frac{\Gamma}{2}t} \right) \right] \exp \left[i \left(\frac{k}{L} \left(x - c\sqrt{\frac{\Gamma}{2}t} \right) + \frac{\omega}{L} \sqrt{\frac{\Gamma}{2}t} \right) \right], \quad (68.a)$$

$$B = \frac{\alpha^2}{\beta(c^2 - 1)} \frac{P^2 + 1}{2LP^3} \tanh \left[\frac{\beta}{L} \left(x - c\sqrt{\frac{\Gamma}{2}t} \right) \right], \quad (68.b)$$

where

$$\alpha^2 = \frac{2(c^2 - 1)}{c^2(c^2 - c_0^2)} (\mu(c^2 - c_0^2) - \omega^2 c_0^2), \quad \beta^2 = \frac{\mu(c^2 - c_0^2) - \omega^2 c_0^2}{(c^2 - c_0^2)^2}, \quad (69.a)$$

$$c_0^2 = \frac{2}{\Gamma} \frac{P^2}{P^2 + 1}, \quad \mu = \frac{2EP^3L^2}{P^2 + 1}, \quad k = \frac{c\omega}{c^2 - c_0^2}. \quad (69.b)$$

The parameter values are given in the caption of Fig. 11. We only show the reconstructed filament, whose shape is computed from the numerical values of A and B according to formula (12) which is accurate to second order in the perturbation parameter.

Our numerical results therefore suggest that traveling pulses are likely to propagate in a stable fashion, at least in some parameter regime. A complete answer to this question would require an analysis of the space- and time-dependent Klein–Gordon equations linearized about a traveling pulse, and is beyond the scope of this paper.

7. Conclusions

This paper gives a detailed description of the dynamics of the coupled nonlinear Klein–Gordon equations, which model an elastic filament subjected to external twist in the vicinity of the first bifurcation threshold. It is shown first that these equations have only two relevant parameters, namely the linear growth rate of amplitude deformations and the ratio of the group velocities of amplitude and twist modulations, and second, that they are Hamiltonian. A complete description of traveling wave solutions to these equations is presented, and localized solutions are identified. Because such solutions are of physical interest, the question of their stability must be addressed. This is accomplished by means of two coupled nonlinear Schrödinger equations, valid in the limit of small amplitude deformations. It turns out that these equations, known as Manakov’s equations, are integrable and arise as a limiting case of model equations describing propagation of light in birefringent fibers or counterpropagating beams in Kerr media. Moreover, since Manakov’s equations are defocusing, their plane wave solutions are modulationally unstable and, as a consequence, traveling holes and fronts of the coupled Klein–Gordon equations have unstable asymptotic states. Interestingly, periodic solutions, which correspond to modulated helical filaments, are also proven to be unstable, and this self-focusing instability is consistent with the looping process observed in elastic rods subjected to excessive twist. It was shown in [25] that, when made unstable, infinite twisted rods tend to first localize deformations and then form twisted loops (eventually giving rise to a braided structure). The analysis of the periodic solutions of CNLKG, therefore, suggests that the formation of loops in finite rods results from a self-focusing instability. Finally, our numerical simulations show that traveling pulses are stable in some parameter regime, but only if the system is kept below threshold.

Acknowledgements

The authors would like to thank N. Ercolani and M. Tabor for many interesting discussions. This work is partly supported by Nato Collaborative Research Grant NATO-CRG 97/037.

Appendix A. Derivation of the nonlinear Schrödinger equations

This section is devoted to a multiple scales analysis of time-independent periodic solutions to the scaled coupled Klein–Gordon equations (14.a) and (14.b). As explained in Section 5, we set

$$A(x, t) = \epsilon A_1(x, T, X_2) + \epsilon^2 A_2(x, T, X_2) + \epsilon^3 A_3(x, T, X_2) + \dots \quad (\text{A.1})$$

$$B(x, t) = \epsilon B_1(x, T, X_2) + \epsilon^2 B_2(x, T, X_2) + \epsilon^3 B_3(x, T, X_2) + \dots \quad (\text{A.2})$$

where $T = \epsilon t$, $X_2 = \epsilon^2 x$, ϵ is a small parameter, and the dots stand for higher order corrections. After substituting in (14.a) and (14.b) and equating like powers in ϵ , we get a hierarchy of partial differential equations which can be solved at each order. At order ϵ , we obtain

$$c_0^2 \frac{\partial^2}{\partial x^2} A_1(x, T, X_2) + \mu A_1(x, T, X_2) = 0, \quad (\text{A.3})$$

$$\frac{\partial^2}{\partial x^2} B_1(x, T, X_2) = 0, \quad (\text{A.4})$$

which gives

$$A_1(x, T, X_2) = F_1(T, X_2)e^{-i\sqrt{\mu}x/c_0} + F_2(T, X_2)e^{i\sqrt{\mu}x/c_0}, \quad (\text{A.5})$$

$$B_1(x, T, X_2) = \kappa, \quad (\text{A.6})$$

where F_1 and F_2 are two complex envelopes and κ is an arbitrary constant. Only the terms which do not lead to divergence at infinity have been kept in B_1 .

At order ϵ^2 , we get

$$\mu A_2(x, T, X_2) + c_0^2 \frac{\partial^2}{\partial x^2} A_2(x, T, X_2) = \left(\frac{\partial}{\partial x} B_1(x, T, X_2) \right) A_1(x, T, X_2) = 0, \quad (\text{A.7})$$

$$\frac{\partial^2}{\partial x^2} B_2(x, T, X_2) = \left(\frac{\partial}{\partial x} A_1(x, T, X_2) \right) A_1^*(x, T, X_2) + A_1(x, T, X_2) \frac{\partial}{\partial x} A_1^*(x, T, X_2). \quad (\text{A.8})$$

After substituting in the expressions for A_1 and its complex conjugate, we can solve for A_2 and B_2 and obtain

$$A_2(x, T, X_2) = 0, \quad (\text{A.9})$$

$$B_2(x, T, X_2) = \frac{ic_0}{\sqrt{2\mu}} \left(e^{-2i\sqrt{\mu}x/c_0} F_2^*(T, X_2) F_1(T, X_2) - e^{2i\sqrt{\mu}x/c_0} F_2(T, X_2) F_1^*(T, X_2) \right). \quad (\text{A.10})$$

We do not include in A_2 and B_2 terms which are in the kernel of the linear operator obtained at order ϵ . These terms have already been taken into account in the expressions of A_1 and B_1 .

At order ϵ^3 , the Klein–Gordon equations read

$$\begin{aligned} & c_0^2 \frac{\partial^2}{\partial x^2} A_3(x, T, X_2) + \mu A_3(x, T, X_2) \\ &= \left(\frac{\partial^2}{\partial T^2} F_1(T, X_2) + |F_1(T, X_2)|^2 F_1(T, X_2) + 2ic_0\sqrt{\mu} \frac{\partial}{\partial X_2} F_1(T, X_2) + |F_2(T, X_2)|^2 F_1(T, X_2) \right) \\ & \times e^{-i\sqrt{\mu}x/c_0} + \left(\frac{\partial^2}{\partial T^2} F_2(T, X_2) + |F_2(T, X_2)|^2 F_2(T, X_2) \right. \\ & \left. - 2ic_0\sqrt{\mu} \frac{\partial}{\partial X_2} F_2(T, X_2) + |F_1(T, X_2)|^2 F_2(T, X_2) \right) e^{i\sqrt{\mu}x/c_0}, \end{aligned} \quad (\text{A.11})$$

$$\frac{\partial^2}{\partial x^2} B_3(x, T, X_2) = 0. \quad (\text{A.12})$$

In order to avoid secular terms in A_3 , we need to impose the two solvability conditions

$$\frac{\partial^2}{\partial T^2} F_1(T, X_2) + |F_2(T, X_2)|^2 F_1(T, X_2) + 2ic_0\sqrt{\mu} \frac{\partial}{\partial X_2} F_1(T, X_2) + |F_1(T, X_2)|^2 F_1(T, X_2) = 0 \quad (\text{A.13})$$

$$\frac{\partial^2}{\partial T^2} F_2(T, X_2) + |F_1(T, X_2)|^2 F_2(T, X_2) - 2ic_0\sqrt{\mu} \frac{\partial}{\partial X_2} F_2(T, X_2) + |F_2(T, X_2)|^2 F_2(T, X_2) = 0, \quad (\text{A.14})$$

which are two coupled nonlinear Schrödinger equations for the envelopes F_1 and F_2 . If we re-write these equations in terms of the original variables x and t and define $F_1'(x, t) = \epsilon F_1(\epsilon t, \epsilon^2 x)$ and $F_2'(x, t) = \epsilon F_2(\epsilon t, \epsilon^2 x)$, we get,

after dropping the primes,

$$\frac{\partial^2 F_1}{\partial t^2} + 2ic_0\sqrt{\mu}\frac{\partial F_1}{\partial x} + |F_1|^2 F_1 + |F_2|^2 F_1 = 0 \quad (\text{A.15})$$

$$\frac{\partial^2 F_2}{\partial t^2} - 2ic_0\sqrt{\mu}\frac{\partial F_2}{\partial x} + |F_2|^2 F_2 + |F_1|^2 F_2 = 0. \quad (\text{A.16})$$

If these equations are satisfied, we can then choose $A_3(x, T, X_2) = 0$ and $B_3(x, T, X_2) = 0$. To order ϵ^3 , the solutions A and B are then given by

$$A(x, t) = F_1(t, x)e^{-i\sqrt{\mu}x/c_0} + F_2(t, x)e^{i\sqrt{\mu}x/c_0} + O(\epsilon^4) \quad (\text{A.17})$$

$$B(x, t) = \kappa + \frac{ic_0}{2\sqrt{\mu}} \left(e^{-2i\sqrt{\mu}x/c_0} F_2^*(t, x)F_1(t, x) - e^{2i\sqrt{\mu}x/c_0} F_2(t, x)F_1^*(t, x) \right) + O(\epsilon^4), \quad (\text{A.18})$$

where we have set $\kappa' = \epsilon\kappa$ and then dropped the prime.

References

- [1] A.E.H. Love, *A Treatise on the Mathematical Theory of Elasticity*, Cambridge University Press, Cambridge, 1892.
- [2] S.S. Antman, *Nonlinear Problems of Elasticity*, Springer, Berlin, 1995.
- [3] A. Goriely, M. Tabor, New amplitude equations for thin elastic rods, *Phys. Rev. Lett.* 77 (1996) 3537–3540.
- [4] E.H. Dill, Kirchhoff's theory of rods, *Arch. Hist. Exact. Sci.* 44 (1992) 2–23.
- [5] B.D. Coleman, E.H. Dill, M. Lembo, Z. Lu, I. Tobias, On the dynamics of rods in the theory of Kirchhoff and Clebsch, *Arch. Rational Mech. Anal.* 121 (1993) 339–359.
- [6] A. Goriely, M. Tabor, Nonlinear dynamics of filaments I: dynamical instabilities, *Physica D* 105 (1997) 20–44.
- [7] A. Goriely, M. Tabor, Nonlinear dynamics of filaments II: nonlinear analysis, *Physica D* 105 (1997) 45–61.
- [8] V.E. Zakharov, S.L. Musher, A.M. Rubenchik, Hamiltonian approach to the description of nonlinear plasma phenomena, *Phys. Rep.* 129 (1985) 286–366.
- [9] A.C. Newell, Finite amplitude instabilities of partial difference equations, *SIAM J. Appl. Math.* 33 (1977) 133–160.
- [10] J. Pedlosky, Finite amplitude baroclinic disturbances in downstream varying currents, *J. Phys. Oceanography* 6 (1976) 335–344.
- [11] J.D. Gibbon, M.J. McGuinness, Amplitude equations at the critical points of unstable dispersive physical systems, *Proc. Roy. Soc. Lond. A* 377 (1981) 185–219.
- [12] E.J. Parkes, The modulational instability of the nonlinear Klein–Gordon equation, *Wave Motion* 13 (1991) 261–275.
- [13] D.J. Benney, A.C. Newell, The propagation of nonlinear wave envelopes, *J. Math. and Phys.* 46 (1967) 133–139.
- [14] S.V. Manakov, On the theory of two-dimensional stationary self-focusing of electromagnetic waves, *Zh. Eksp. Teor. Fiz.* 65 (1973) 505–516.
- [15] S.V. Manakov, On the theory of two-dimensional stationary self-focusing of electromagnetic waves, *Sov. Phys. JETP* 38 (1974) 248–253.
- [16] J. Yang, Classification of the solitary waves in coupled nonlinear Schrödinger equations, *Physica D* 108 (1997) 92–112.
- [17] D.J. Muraki, W.L. Kath, Hamiltonian dynamics of solitons in optical fibers, *Physica D* 48 (1991) 53–64.
- [18] W.J. Firth, A. Fitzgerald, C. Paré, Transverse instabilities due to counterpropagation in Kerr media, *J. Opt. Soc. Am. B* 7 (1990) 1087–1097.
- [19] M. Haelterman, A.P. Sheppard, A.W. Snyder, Bimodal counterpropagating spatial solitary-waves, *Optics Communications* 103 (1993) 145–152.
- [20] O.C. Wright, Modulational instability in a defocusing coupled nonlinear Schrödinger system, *Physica D* 82 (1995) 1–10.
- [21] Y.A. Li, K. Promislow, Stability and Structural stability of non-ground state traveling waves of coupled nonlinear Schrödinger equations, *Physica D*, 1998, submitted for publication.
- [22] A. Goriely, M. Tabor, Spontaneous helix-hand reversal and tendril perversion in climbing plants, *Phys. Rev. Lett.* 80 (1998) 1564–1567.
- [23] R.L. Higdon, Radiation boundary conditions for dispersive waves, *SIAM J. Num. Anal.* 31 (1994) 64–100.
- [24] S.K. Lele, Compact finite difference schemes with spectral-like resolution, *J. Computational Phys.* 103 (1992) 16–42.
- [25] A. Goriely, M. Tabor, Nonlinear dynamics of filaments IV: spontaneous looping of twisted elastic rods, *Proc. Roy. Soc. London (A)* 45 (1998) 3183–3202.